A simplified null-point method for high resolution contact temperature measurement by means of micro-thermocouples in vacuum conditions

L. Thiery*, J.Y. Rauch, S. Euphrasie and B. Cretin
Université Marie et Louis Pasteur, CNRS, institut FEMTO-ST, F-25000 Besançon, France

Abstract: We report on the possibility to measure the temperature of micro-devices by means of a micro-thermocouple in active mode with a simplified procedure of null-point method. Contrary to other reported procedures, there is no need of multiple scans at different distances to the sample surface. A single out of contact power calibration is required prior to the contact-point measurements. For them, only two successive measurements at different Joule heating powers of the thermocouple are necessary to deduce the actual surface temperature. We only used a low frequency voltage generator and high precision voltmeters without specific electronics except a low-pass RC filter. The reliability of the method is demonstrated with a platinum wire as a calibration tool.

Keywords: temperature measurement, micro-thermocouple, contact surface temperature, null-point, active mode.

Nomenclature:

General		Index and suffix
d: diameter	I: RMS current	i: material index, 1 for platinum and 2 for platinum-10% rhodium alloy
L: length of one wire	P: input Joule power	j: discretized element of i wire
S: wire cross section	h: radiative surface heat transfer coefficient	tj: thermocouple junction
p: wire perimeter	g: thermal conductance	nc: no-contact
x: coordinate along a wire	σ_x: standard deviation on x data	c: contact
ρe: electrical resistivity	T: temperature at x position in the wire	cc: cold contact
α: temperature coefficient of resistance	T_a ambient temperature	hc: hot contact
ε: emissivity	$\theta = T - T_a$: temperature difference with ambient	e: external
k: thermal conductivity	q: heat power	s: surface

1. Introduction

Surface temperature measurement with high spatial resolution remains a major issue especially in vacuum conditions. In a previous article, we described the different available techniques that can be broadly classified in two groups: conventional or non-contact and near-field or contact techniques [1]. We recalled that non-contact techniques are limited in terms of spatial resolution, temperature range and their dependence on the surface optical nature whereas contact techniques overcome part of these drawbacks. Consequently, the only way to reach high spatial resolution requires the use of a local probe such as used in all the near-field techniques. Unfortunately, the latter are subjected to discrepancies related to the effect of thermal diffusion between the sample and the sensor which becomes the main error source. We presented the potential of thermocouple micro-probes as a relevant alternative to available thermal probes for Scanning Thermal Microscopes (SThM) which are derived from Atomic Force Microscope (AFM) probes where a thermal sensitive area is added to provide additional information related to heat transfer between this area and the sample. Two modes are available for temperature or thermal conductance measurements, namely TCM (temperature contrast mode) and CCM (conductivity contrast mode) respectively [2,3]. The specific case of passive mode for temperature measurement on a sample surface was described and a specific calibration procedure was developed [1]. It was demonstrated that it is impossible to measure surface temperature with a high level of accuracy since one cannot predict and estimate the different thermal resistances involved in the measurement on any object. Classically, these are the probe resistance (R_p), the contact resistance (R_c) between the probe tip and the surface and the spreading resistance in the object itself (R_s).

Here, we present the use of the same kind of thermocouple probe for measuring contact temperature at sub-micron-scale in a vacuum chamber by means of the active method, also called the “null-point” method which is an extension of the double-scan technique developed to get rid of parasitic heat exchanges effects around the SThM probe [4,5]. However, as clearly explained by the authors, this does not prevent the effect of heat diffusion inside the sample itself and the

* corresponding author: laurent.thiery@univ-fcomte.fr

resulting disturbances. The main difficulty in the double scan technique relies on the extraction of the jump temperature between contact and no-contact, the latter being extrapolated from two scans at different height from the surface. Double-scan then becomes triple-scan: a first to obtain contact temperature and surface profile and two scans at different heights. Null-point method has extended the double-scan technique by adding an active operation mode [6]. In this mode, the thermocouple is heated by alternative current (AC) with Joule effect at a sufficiently high frequency for insuring a complete vanishing of thermal AC components in the thermoelectric signal. The direct current (DC) component of the temperature is then measured for thermal conductivity extraction or/and actual surface temperature. The described method shows that for the use of a standard SThM thermocouple probe in scanning mode, 6 scans are necessary to calculate the actual surface temperature in atmospheric pressure [7,8]. In vacuum, this reduces to 2 scans due to absence of heat transfer in the surrounding gas and the direct access to non-contact temperature value [9]. However, in both cases, the different contact scans are supposed to be strictly identical in terms of strength and geometry so that the thermal contact resistance and the spreading one are the same for each measurement location. This point can be subjected to discussion since the probability to pass 2 times strictly on the same points with the same contact configuration cannot be 100%. A simple change in the tip shape due to wear or damage between both scans may affect these two resistances. Consequently, the possibility to obtain the required data at each point at one time, is the only way to resolve the issue of multiple scans, despite a significant increase in scanning time. This why we propose a new method to reduce the number of scans. It consists in the exploitation of the linear behaviour of the measured junction temperature of the thermocouple probe regarding supplied heat power in both contact and non-contact mode. From the measurements of both slopes, it is possible to extrapolate the actual surface temperature. Only a single out of contact power calibration before and only one scan with two successive measurements at different Joule heating powers of the thermocouple are necessary. We demonstrate the reliability of this technique using a calibration procedure on a platinum wire whose contact temperature is known within 3 K.

The micro-thermocouple probe is first presented along with a modelling describing the temperature along its wires and this model limitations. Then our new simplified null-point procedure in vacuum is explained and described. We then present our experimental set-up before showing the results and discussing them.

2. Micro-thermocouple probe

2.1 Fabrication and dimension characterization

A micron-size S type thermocouple is used, made with Wollaston 1.27 µm diameter wires of platinum and platinum-10% rhodium. They are mainly used as Scanning Thermal Microscope (SThM) probes for both passive and active local sensors [10,11]. For that purpose, the thermocouple junctions are systematically reshaped by means of a focused ion beam (FIB) in order to refine the tip apex and optimize the probe spatial resolution. Fig. 1 presents the thermocouple junction used in the present article. Fig. 1a shows a large view of the thermocouple made of two Wollaston wires. Silver claddings are visible and the stripped lengths of platinum and platinum-10% rhodium are the same, approximately 300 µm. They seem dissymmetric only due to the view angle and the large field depth of the electron beam. Fig. 1b depicts the junction after FIB reshaping. The measured diameters of the wires are 1.29 and 1.24 µm for the platinum and platinum-rhodium alloy respectively. The increase of the diameter of the upper wire (platinum-rhodium) is probably due to a local fusion during welding; this does not affect the junction behaviour and may only contribute to the slight difference between measurements and calculations as seen below.

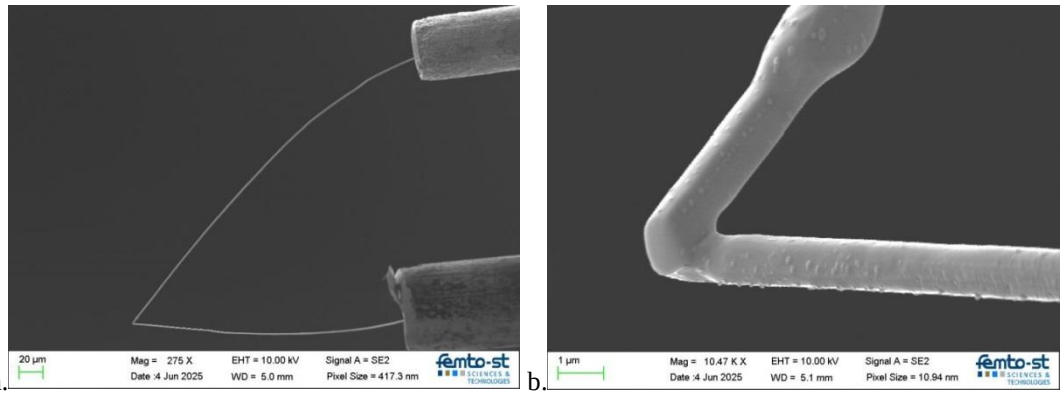

Fig. 1. S type micro-thermocouple used in this article: a) overall view, b) junction after reshaping by FIB.

One of the advantages of the use of a wire thermocouple relies on its geometry simplicity regarding usual SThM cantilever probes. It is then easy to model its behaviour in different modes.

2.2 Modelling of temperature along the thermocouple wires

In vacuum null-point (VNP) method [9], the thermocouple is heated by Joule effect in AC mode. It is similar to 2ω mode except the current frequency is increased above its thermal cut-off frequency to extract only the DC temperature, which can be provided by a simple low-pass filter. In 2ω mode, we can assume that temperature dependence of electrical resistivity and material thermophysical parameters are constant values as long as the magnitude of the 2ω temperature component is on the order of a few degrees [12]. Furthermore, the assumption of a single material using mean values of thermal and electrical characteristics of both wires was also acceptable to match experiments. However, in active mode used for temperature measurement, such simplifications cannot be acceptable anymore since the temperature range goes from ambient to several hundreds of degrees. In addition, even if no convection occurs in vacuum, radiative heat transfer must be taken into account. Consequently, the mathematical problem becomes non-linear and only a few methods can be applied to solve it. We have chosen to keep linear expression of differential equation of heat into portions of wire whose solutions are known for each discretized element. Furthermore, radiative heat transfer can be linearized and introduced as a surface heat transfer coefficient h. Both wires are discretized in *n* portions, each of them being defined with their own thermal and electrical parameters that depend on the temperature. The *2n* integration constants of the obtained system of equations are resolved numerically using boundary conditions. For this, let us consider the thermocouple as a junction of two wires at the axis origin x = 0, a platinum wire on one side of index i = 1, and platinum-10%rhodium on the other side of index i = 2, as shown in Fig. 2. Each wire is discretized in n elements, from j=1 to j=n. Due to the very small diameter of wires, a section is thermally homogeneous so that the temperature distribution only depends on the longitudinal direction x. A simple Biot number estimation could demonstrate this assertion.

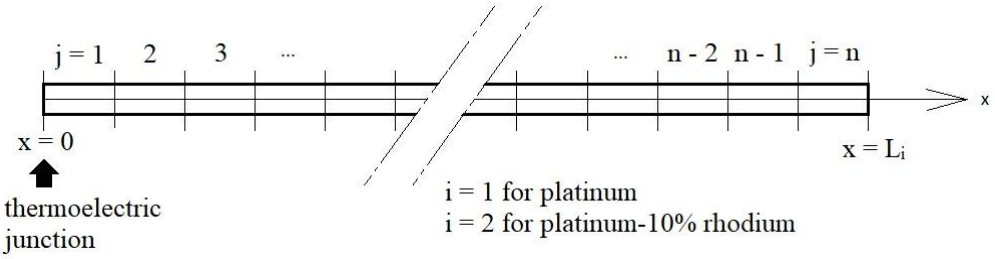

Fig. 2. Modelling principle of each wire starting from the junction location x = 0, made of n elements.

Each of these n elements is thermally governed by the same differential equation written in steady-state:

$$k_{i,j}S_i\frac{d^2T_{i,j}}{dx^2}dx + h_{i,j}p_i\left(T_a - T_{i,j}\right)dx + \frac{\rho e_{i,j}dx}{S_i}I^2 = 0 \qquad (1)$$

in which i = 1 for platinum, and i = 2 for platinum-10% rhodium wires.

Section S_i and perimeter p_i are given for the same wire, not strictly equals as shown below. $h_{i,j}$ represents the external surface radiative heat transfer coefficient. $k_{i,j}$ and $\rho e_{i,j}$ are the thermal conductivity and electrical resistivity of the considered element respectively. Their values are temperature dependent but are assumed as homogeneous in each element.

$T_{i,j}$ is the steady temperature at a location x into the element (i,j) that results from the thermal balance in which I corresponds to the RMS current value at the ω radial frequency. The linearized radiative surface heat transfer coefficient h_i is calculated from the element temperature $T_{i,j}$ and the ambient value T_a, such:

$$h_{i,j} = \varepsilon\sigma\left({T_{i,j}}^2 + {T_a}^2\right)\left(T_{i,j} + T_a\right) \qquad (2)$$

Stefan-Boltzmann constant is $\sigma = 5.67\ 10^{-8}$ W.m^{-2}.K^{-4} and ε is the emissivity of the materials assumed as constant for both materials and chosen as 0.14. This value corresponds to the best fitting value for platinum wire in the same condition as described in the section 3. It will be shown below that this value has no major effect on the thermocouple temperature distribution. We also assume that the emissivity of platinum-10% rhodium is the same.

By changing the temperature with $\theta_{i,j} = T_{i,j} - T_a$, and introducing $m_{i,j} = \sqrt{\frac{h_{i,j}p_i}{k_{i,j}S_i}}$, the equations become:

$$\frac{d^2\theta_{i,j}}{dx^2} - m_{i,j}^2\,\theta_{i,j} = -\frac{\rho e_{i,j}}{k_{i,j}S_i^2}I^2 \qquad (3)$$

And their solutions in which section S_i and perimeter p_i are replaced with their formulae depending on the wire diameter d_i:

$$\theta_{i,j} = \left(\frac{2I}{\pi}\right)^2 \frac{\rho e_{i,j}}{h_{i,j}\, d_i^3} + A_{i,j} e^{m_{i,j}\, x} + B_{i,j} e^{-m_{i,j}\, x} \qquad (4)$$

Constants $A_{i,j}$ and $B_{i,j}$ are obtained numerically from boundary conditions expressing continuity of temperature and heat flux.

At x = 0, junction temperature equality gives: $\theta_{1,1}(0) = \theta_{2,1}(0)$ (5)

When the junction is in contact with the sample surface at the temperature T_s, $\theta_s = T_s - T_a$ and the thermal balance gives:

$$k_{1,1} S_1 \left.\frac{d\theta_{1,1}}{dx}\right|_{x=0} + k_{2,1} S_2 \left.\frac{d\theta_{2,1}}{dx}\right|_{x=0} + g\left(\theta_{2,1}(0) - \theta_s\right) = 0 \qquad (6)$$

In this expression, g is the contact thermal conductance between the tip and the sample surface.

This condition assumes that the welded junction is perfect, without any additional resistance due to a possible contact defect. This is justified by the junction quality shown in Fig. 1a, and the matching between measured resistance and the calculated one using measured dimensions.

At each element boundary, temperature and heat flux continuities give:

$$\theta_{i,j}\left(j\frac{L_i}{n}\right) = \theta_{i,j+1}\left(j\frac{L_i}{n}\right) \quad \text{and} \quad k_{i,j} S_i \left.\frac{d\theta_{i,j}}{dx}\right|_{x=j\frac{L}{n}} = k_{i,j} S_i \left.\frac{d\theta_{i,j+1}}{dx}\right|_{x=j\frac{L}{n}} \qquad (7)$$

for i =1 and 2; j = 1, 2, …, n – 1.

At the end of the wires, where $x = L_i$, the 75 µm diameter silver cladding is sufficiently massive and thermally conductive to remain at ambient temperature T_a, so that:

$$\theta_{1,n}(L_1) = \theta_{2,n}(L_2) = 0 \qquad (8)$$

In the following results, geometrical data have been measured by means of a scanning electron microscope. Measurements have been performed in vacuum. Table 1 presents the different data used for the calculations. Due to their negligible influence on the results, we have used constant thermal conductivities for both platinum and platinum-10% rhodium alloy [13]. Consequently, $k_{i,j}$ becomes k_i as given in Table 1. The electrical resistivity is corrected using their temperature coefficient of resistance α_i and the linear relation [14]:

$$\rho e_{i,j} = \rho e_i(T_a)\left(1 + \alpha_i \theta_{i,j}\right) \qquad (9)$$

Results are obtained with an iterative procedure in which electrical resistivity and radiative surface heat transfer coefficient are corrected according to the reached element temperature until it remains unchanged. Depending on the temperature level, the number of iterations is typically between 4 and 10. We have fixed the number of discretized elements to 20 per wire, which represent a length of about 20 µm per element. We verified that 10 elements only were sufficient to provide the same results.

Table 1. Thermocouple wires characteristics.

Platinum					Platinum-10% rhodium				
d_1 (µm)	L_1 (µm)	k_1 ($W.m^{-1}.K^{-1}$)	$\rho e_1(T_a)$ ($\Omega.m$)	α_1 (K^{-1})	d_2 (µm)	L_2 (µm)	k_2 ($W.m^{-1}.K^{-1}$)	$\rho e_2(T_a)$ ($\Omega.m$)	α_2 (K^{-1})
1.29	300	72.5	$10.5\ 10^{-8}$	$3.85\ 10^{-3}$	1.24	300	38	$18.8\ 10^{-8}$	$1.7\ 10^{-3}$

Once the temperature distribution has been calculated, the junction value can be extracted and plotted versus the Joule power, which corresponds to the product of the squared RMS current I^2 and the total thermocouple resistance, which is the sum for each element:

$$R = \frac{L_1}{n\, S_1}\left(\sum_{j=1}^{n} \rho e_{1,j}\right) + \frac{L_2}{n\, S_2}\left(\sum_{j=1}^{n} \rho e_{2,j}\right) \qquad (10)$$

An example of temperature distributions along the thermocouple wires is presented in Fig. 3. Input current is set to 1.2 mA and three curves are depicted: “no-contact”, “cold-contact” ($\theta_s = 0$), and “hot-contact” ($\theta_s = 300$ K). Platinum is on the left negative x locations whereas platinum-10% rhodium is on the right positive. The maximum temperature is reached in this wire due to its higher electrical resistivity and also on its lower thermal conductivity. In spite of this dissymmetry, the provided thermoelectric voltage corresponds to the junction temperature. Each discretized element is visible in red and blue colours successively in this figure.

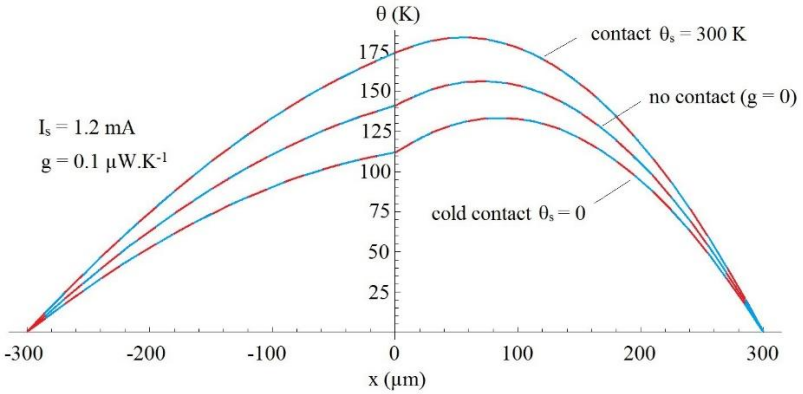

Fig. 3. Temperature distribution along the thermocouple, for an RMS current of 1.2 mA, for which Joule power equals 126 µW. The computation was done using 20 elements per wire.

In Fig.3, and all the following results, the number of elements per wire is 20. We have verified that this number is sufficient, as shown in Fig. 4 in which the temperature increase of the junction is plotted versus the input Joule power for different number values, from 1 to 50. We notice that 5 elements provide the same results than 50 elements.

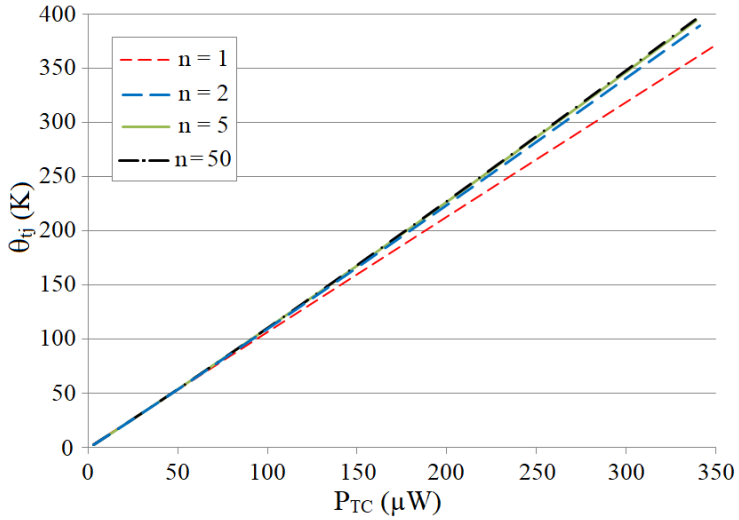

Fig. 4. Thermocouple junction temperature calculations versus power input for different element numbers.

In this figure, the important point to be noticed relies on the linearity of the temperature response versus the supplied Joule power. Measurements confirm this shape for moderate level of temperature as shown below.

2.3 Model limitations

A first source of deviation of this model is related to the homogeneous Dirichlet condition at the extremity of the wires. Such a condition requires some clarifications since in vacuum, the cold sink is only due to conductive heat diffusion so that the ambient temperature could be found much farther than supposed. Fig. 5 depicts a large view of the thermocouple which includes the silver leads and the ceramic holder in which the wires are introduced and glued. The thermocouple cold junction is materialized at the interface between Pt and Pt-Rh wires and silver, as shown by θ_{left} and θ_{right}.

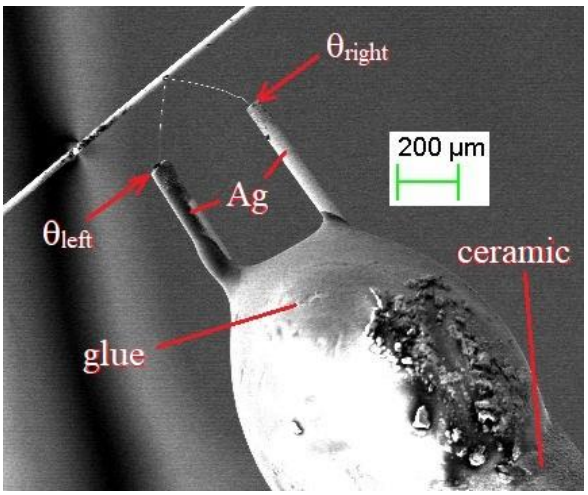

Fig. 5. Overview of the thermocouple inside his ceramic holder.

Free length of silver is about 500 µm before a drop of glue and the ceramic tube. Silver total lengths are 3 cm before their welding with tin on copper contacts. Ambient temperature is measured by a Pt100 probe on the basement of the ceramic tube. This means that ambient temperature occurs somewhere in this area.
Let us consider two cases of location for ambient temperature: at the glue (500 µm) and at a distance of 1 mm into the ceramic tube which may be considered as the realistic one. The condition then becomes a heat flux condition (Neumann) for which a thermal conductance g_L is involved so that:

$$-k_1 S_1 \frac{d\theta_{1,n}}{dx} = g_L \theta_{1,n}(L_1) = g_L \theta_{left}$$

and $$-k_2 S_2 \frac{d\theta_{2,n}}{dx} = g_L \theta_{2,n}(L_2) = g_L \theta_{right}$$

The thermal conductance g_L depends on the silver wire length such as: $$g_L = \frac{k_{Ag} S_{Ag}}{L_{Ag}}$$

S_{Ag} and L_{Ag} are the cross section and the considered length of the silver cladding to reach ambient temperature respectively. Silver thermal conductivity is around 420 $W.m^{-1}.K^{-1}$ and the wire diameter is 75 µm. As a result, values of g_L are 3.7 10^{-3} $W.K^{-1}$ and 1.85 10^{-3} $W.K^{-1}$ for 500 µm and 1 mm length respectively. Fig. 6 depicts the resulting cold temperature at the interface location θ_{left} and θ_{right} that remain typically below a tenth of degree. This is negligible since the junction temperature increase is 400 K at the maximum power of 350 µW. Besides, the important point is that the absolute temperature of the junction increases of a quantity that is of the same order of θ_{left} and θ_{right}. As a result, the Seebeck voltage which represents the temperature difference between the hot junction and the cold one does not change.

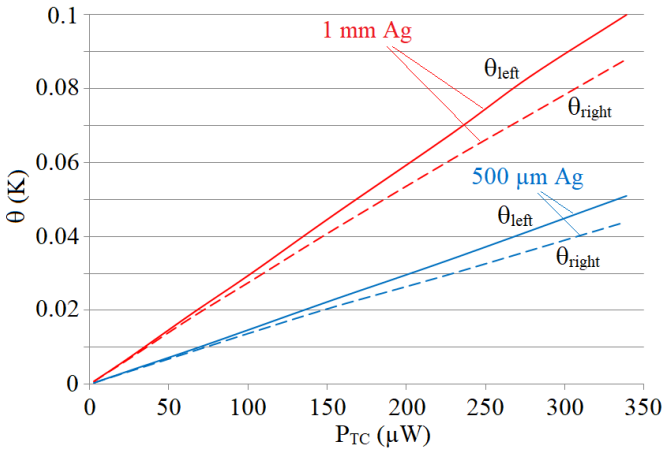

Fig. 6. Temperature elevation at the wire extremities (cold thermocouple reference) for two Neumann conditions.

This means that even taking into account such deviation will hardly change the result. It leads to an uncertainty of the hot junction temperature below 0.1K. Unfortunately, knowing precisely the cold junction temperature remains presently not possible.

Let us now focus on the junction temperature given by the Seebeck voltage versus the supplied Joule power which is the key point of our analysis. In the following results, the thermocouple junction temperature is noted T_{tj} at the location x = 0 (tj stands for thermocouple junction), and the difference with ambient temperature: $\theta_{tj} = T_{tj} - T_a = \theta(0)$.
The calculated temperature given by the thermocouple varies quasi-linearly versus the Joule dissipated power, noted P_{TC}. Fig. 7 compares measurements given by the thermocouple junction and calculations. As mentioned above, model calculations given with Dirichlet or Neumann conditions provide nearly identical results. The straight black line depicted in Fig. 7 points out the slight deviation from linearity of both modelling and measurements.

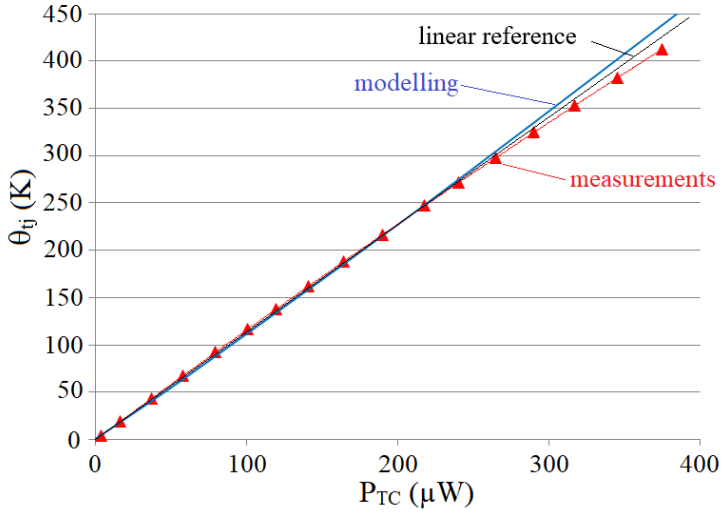

Fig. 7. Modelling and measurement deviation from linear in non-contact mode.

The curvature difference cannot be explained by a possible increase of the emissivity because of the limited length of the thermocouple wires. Indeed, if we consider the Joule power of Fig. 3 with a RMS current of 1.2 mA, the total supplied Joule power is 126.1 µW. We calculated that conduction of heat from the wire extremities to the silver is 125.8 µW (65.5 µW from platinum wire and 60.3 µW from the platinum-10% rhodium wire). This means that radiation loss is only 0.3 µW so that the effect of emissivity remains almost negligible except at very high temperatures. As a result, the relationship between junction temperature and the supplied power is driven by conduction into silver cladding so that the difference could be explained by both the moderate increase of thermal conductivities in addition to the slight deviation of the TCR from linearity whose value decreases when the temperature increases. However, the linear approximation is good enough to obtain reliable results.
Anyway, considering measurements values as the actual junction temperature, a few points are enough to extract a linear fit whose slope is the key point since it is dependent on the thermal balance of the junction.

3. New null-point technique explications and procedure

In non-contact mode as shown in Fig. 7, the slope is maximum compared to contact mode. The slope decreases when more heat dissipates from the junction, in particular when the contact conductance increases. This is shown in Fig. 8, where the model has been used to compare the effect of different thermal contact conductance. On a cold surface, the heat power required to reach the same temperature is higher as shown with the red line (cold contact). The applied contact thermal conductance g corresponds to the experimentally fitted values presented in the results section, with a value of 0.1 µW K^{-1}.

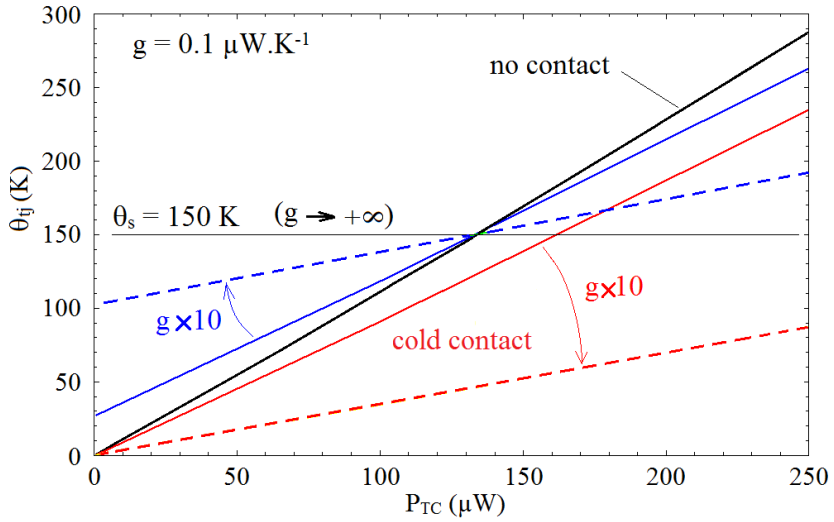

Fig. 8. Thermocouple junction temperature versus input power for different cases of contact and no-contact (black line): cold contact in red lines and hot contact in blue lines.

When a contact occurs on a hot surface θ_s >0, this changes the amount of power needed to reach the same level of temperature. However, if the contact conductance g remains identical, the temperature versus power slope is unchanged (blue line). Indeed, blue and red lines are strictly parallel, which will be demonstrated latter. The given example is a surface at 150 K above ambient. As long as the junction temperature is lower than the surface one, heat flows from the surface to the junction. Inversely, when the junction temperature is higher than the surface one, the heat flux is reversed and the surface is heated up by the thermocouple. When junction and surface are in thermal equilibrium, there is no heat transfer so that the junction temperature is the same that in the case of no contact which corresponds to the crossing point between contact and no contact responses. This crossing point is not modified when the contact conductance changes, as shown by the dashed lines for which g value has been increased by an order of magnitude. The dashed red line corresponds to a cold contact, whereas the dashed blue one corresponds to a hot contact on the 150 K hot surface. The limit case of a perfect contact ($g \to +\infty$) would lead to the horizontal black thin line for which junction temperature equals surface temperature independently to the supplied power to the thermocouple.
Consequently, once the *no contact* response of the probe is extracted from a power ramp, there are two options:

- by assuming an invariant contact conductance g, a cold contact ramp response provides the slope from which a single scan at a given power is enough to extrapolate the surface temperature,
- if the contact conductance g is expected to change when scanning the surface of the sample, at least two (or more) power response per each contact point can provide the extrapolated actual surface temperature.

The second option is preferred since, in the general case and as seen below, the contact conductance is hardly predictable when contacting any surface object. Then, it is only possible to take advantage of the linearity of the thermocouple response for an accurate extraction of the crossing point temperature.

As shown in Fig. 8, when the thermocouple is in contact with a surface, the extraction of the slope of its temperature versus the supplied power allows to deduce the actual surface temperature given by the crossing point with the non-contact temperature response.
The observed linearity can be explained by a simple 0-D description of a thermocouple junction at a homogeneous temperature whose value results from the heat balance between external and contact conductances, g_e and g_c respectively. The Joule power supplied to the thermocouple, noted q, dissipates from the wires to ambient surrounding depending on the contact or not. Without contact (nc suffix), the thermal balance of the junction area is governed by the equality:

$$q = g_e\, \theta_{tj}^{nc} \qquad (11)$$

g_e is the thermal conductance to external ambient source, mainly by conduction to the thermocouple support, and eventually by radiation. When a contact occurs with a surface at temperature T_s (c suffix), q power is the sum of the external heat dissipation q_e and the tip-to-sample heat diffusion q_{ts} so that the heat balance gives:

$$q = q_e + q_{ts} = g_e\theta_{tj}^{c} + g_c\left(T_{tj} - T_s\right) = (g_e + g_c)\theta_{tj}^{c} - g_c\theta_s \qquad (12)$$

where $\theta_s = T_s - T_a$ and the tip-to-surface contact conductance is g_c.

The case of a *cold contact* (cc suffix) for which T_s equals T_a leads to the simplified expression:

$$q = (g_e + g_c)\theta_{tj}^{cc} \quad (13)$$

As we measure the thermocouple value versus the Joule power q, let us reverse the heat balance to extract the slopes as depicted in Fig. 9. The non-contact ramp gives: $\theta_{tj}^{nc} = \frac{q}{g_e} = aq$ (14)

Then, the cold contact ramp provides the response: $\theta_{tj}^{cc} = \frac{q}{g_e+g_c} = bq$ (15)

And the hot contact ramp gives: $\theta_{tj}^{hc} = \frac{q}{g_e+g_c} + \frac{g_c\,\theta_s}{g_e+g_c} = bq + \theta_0$ (16)

which shows why the red and blue curves in Fig. 8 are parallel, with the same slope b.

However, when considering a different contact conductance g_c', a contact ramp on the hot surface (hc suffix) leads to:

$$\theta_{tj}^{hc} = \frac{q}{g_e+g_c'} + \frac{g_c'\,\theta_s}{g_e+g_c'} = b'q + \theta'_0 \quad (17)$$

It follows that the actual surface temperature is deduced from the crossing-point at a power q_s for which the heat flux between the thermocouple junction and the surface is null and $\theta_{tj} = \theta_s$ and then:

$$\theta_s = aq_s = b'q_s + \theta'_0 \quad (18)$$

So that: $q_s = \frac{\theta'_0}{a-b'}$ (19)

and then: $\theta_s = \frac{a\,\theta'_0}{a-b'}$ (20)

As a result, a minimum of two values are required to extract the slope b' at a given location. Finally, the procedure could be this:

- firstly, the *no contact* measurement with different power values is required to provide the value *a* from the slope,
- secondly, as depicted in Fig. 5, two different powers are used when in contact, giving θ_1 and θ_2 junction temperatures at the powers q_1 and q_2 respectively. Both constants b' and θ'_0 are then obtained as: $b' = \frac{\theta_1-\theta_2}{q_1-q_2}$ and $\theta'_0 = \theta_1 - \frac{\theta_1-\theta_2}{q_1-q_2}q_1$ from which the surface temperature θ_s can be deduced from equation (20).

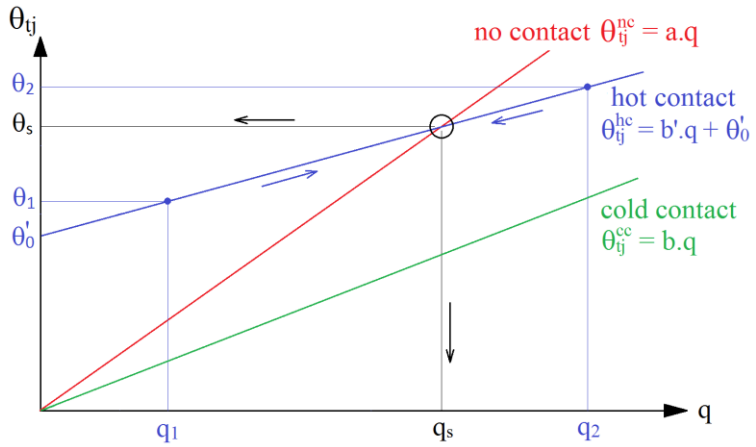

Fig. 9. Method for extrapolating the surface temperature using two contact points.

This procedure is then quite simple: after having extracted the temperature response without contact, two values in contact mode should allow deducing the surface temperature. It is worth noting that increasing the number of data points reduces the uncertainty, as the slope is determined using a least square fitting method. Let us evaluate the uncertainties in the extraction of the surface temperature regarding the number of measured points.

For these measurements, we used a Keithley 2000 as a multimeter with an accuracy better than 0.01%. The standard deviation of the temperature measurements is estimated to be better than 0.5 K. The uncertainty of the measured power is small compared to the uncertainty of the measured thermoelectric effect and will be neglected to obtain the uncertainty of θ_s. We could have used the York algorithm [15] if we wanted to take into account the uncertainty of the measured power to compute the standard deviation of the slope and the intercept of a linear regression. As the points near the intersection of the 2 curves are more important, we can use a weighted least squares (WLS) fitting. For the contact curves, we chose a Gaussian distribution for the weights w_i depending on its Euclidean distance ED_i from an intersection point (x_0, y_0) obtained with a regular unweighted linear regression:

$$ED_i = \sqrt{(x_i - x_0)^2 + (y_i - y)^2} \quad (21),$$

$$w_i = exp\left(-\left(\frac{ED_i}{2\overline{ED}}\right)^2\right) \quad (22),$$

with (x_i, y_i) the points of the contact curves et $\overline{ED}$ the mean of ED_i. The weights were then normalized so that their sum equals the number of points.

For a normal distribution of n points, with n>2, the unbiased standard error estimator of the slope *b* obtained by a WLS linear regression is [16]:

$$\sigma_b = \sqrt{\left(\frac{1}{n-2}\sum_{i=1}^{n} w_i \varepsilon_i^2\right) / \left(\sum_{i=1}^{n} w_i \sum_{i=1}^{n} x_i^2 - \sum_{i=1}^{n} w_i x_i^2\right)} \quad (23),$$

where ε_i is the error of y_i compared to the obtained WLS linear regression. In the case the intercept is 0 (for the non-contact measurement), with no weight, it becomes:

$$\sigma_a = \sqrt{\left(\frac{1}{n-1}\sum_{i=1}^{n} \varepsilon_i^2\right) / \left(\sum_{i=1}^{n} (x_i)^2\right)} \quad (24)$$

For only two points with a standard deviation σ (σ = 0.5K for computations in Table 2) for y_i, the standard deviation of the slope is

$$\sigma_b = \sqrt{2}\sigma / |x_2 - x_1| \quad (25).$$

For the contact curves, the standard error estimator of the intercept θ_0 is:

$$\sigma_{\theta 0} = \sigma_b \sqrt{\left(\sum_{i=1}^{n} w_i x_i^2\right) / \left(\sum_{i=1}^{n} w_i\right)} \quad (26).$$

The covariance between the slope b and the intercept θ_0 is:

$$cov(b, \theta_0) = -{\sigma_b}^2 \left(\sum_{i=1}^{n} w_i x_i\right) / \left(\sum_{i=1}^{n} w_i\right) \quad (27).$$

Neglecting the correlation between the errors of the slope a (of the non-contact measurements) with the errors of the slope b (of the contact measurements) and its intercept θ_0, the standard deviation of the object temperature θ_s is:

$$\sigma_{\theta s} = \sqrt{\left(\frac{a\sigma_{\theta 0}}{a-b}\right)^2 + \left(\frac{a\theta_0\sigma_b}{(a-b)^2}\right)^2 + 2\left(\frac{a}{a-b}\right)\left(\frac{a\theta_0}{(a-b)^2}\right) cov(b, \theta_0) + \left(\frac{b\theta_0\sigma_a}{(a-b)^2}\right)^2} \quad (28)$$

To validate this procedure, the next part presents a calibration approach. It uses one of the simplest and most reliable calibration devices, which is a platinum wire.

4. Calibration wire in vacuum conditions

Platinum wires are very good candidates for calibration process due to their linear behaviour and insensitivity to oxidation and impurities at high temperature. They also possess the advantage of being compatible with high temperatures in vacuum. A wire is also preferable to thin-film devices for which the electrical and thermal characteristics can significantly differ from bulk values and the thermal dependence to a substrate may disturb the thermal equilibrium so that the actual surface temperature could be suspected to large discrepancies. A simple cylindrical wire is also easy to model with the same method used for the thermocouple in the previous section.

Let us consider a single platinum wire to be discretized identical to the platinum wire of the thermocouple. The solution is exactly the same than expression (4):

$$\theta_j = \left(\frac{2I}{\pi}\right)^2 \frac{\rho e_j}{h_j d^3} + A_j e^{m_j x} + B_j e^{-m_j x} \quad (29)$$

For each element j, the temperature is given by $\theta_j = T_j - T_a$ and $m_j = \sqrt{\frac{h_j p}{k S}}$. The diameter is a constant so that p and S are constant values for perimeter and section respectively. The thermal conductivity is also assumed constant (72.5 $W.m^{-1}.K^{-1}$) since we have verified that taking into account its temperature dependence had no significant effect on the wire temperature distribution.

The thermocouple junction is subjected to be put in contact with the wire at the hottest location which is the centre. Furthermore, at the extremity of the wire, the temperature is kept at ambient conditions due to a massive tin welding on the copper leads. The problem is then symmetrical so that the axis origin, x = 0, is located at the centre of the wire and only a half-length is relevant to study.

Then, the condition at the contact point is expressed as:

$$2k_1 S \left.\frac{d\theta_1}{dx}\right|_{x=0} = g(\theta_1(0) - \theta_c) \quad (30)$$

where g is the contact conductance and θ_c is the temperature elevation of the contacted object, here the thermocouple junction. At each element boundary, temperature and heat flux continuities give:

$$\theta_j\left(j\frac{L_i}{n}\right) = \theta_{j+1}\left(j\frac{L_i}{n}\right) \quad \text{and} \quad k_j S \left.\frac{d\theta_j}{dx}\right|_{x=j\frac{L}{n}} = k_{j+1} S \left.\frac{d\theta_{j+1}}{dx}\right|_{x=j\frac{L}{n}} \quad (31)$$

for j = 1, 2…, n – 1.

At the extremity of the wire, for x = L, there is no temperature elevation, therefore: $\theta_n(L) = 0$ (32)

In the following results, we have fixed values as 25.2 µm using measurement of the diameter (see Fig. 8), its resistance at ambient temperature (14.95 Ω) for which the half-length L gives 35.6 mm and the emissivity ε value for the best fit on measured points as 0.14.

An example of the temperature distribution along the wire is depicted in Fig. 10, for a DC current of 8.8 mA. The Joule power is 1.64 mW and the effect of the contact is made visible by setting the contact conductance g to a large value of 2 µW K^{-1}. Actual value of the thermocouple contact is on the order of 0.1 µW K^{-1} as shown in Fig. 3 and the following results. However, this value would not have produced significant change on the wire temperature distribution.

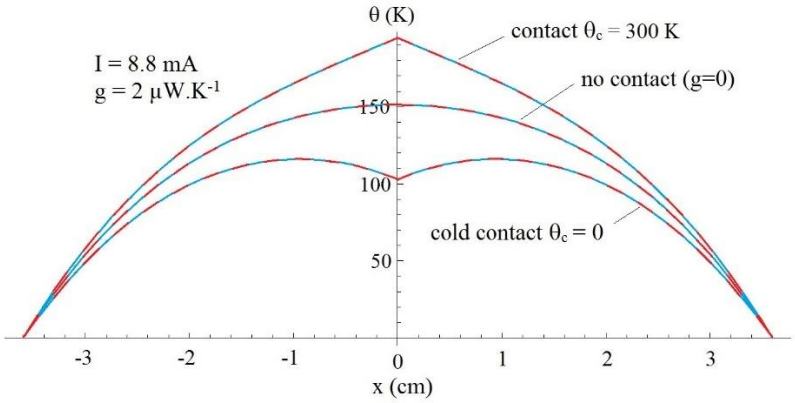

Fig. 10. Temperature distribution along the platinum wire for a current of 8.8 mA, for different contact situations and a contact conductance 20 times higher than the thermocouple one.

During the calibration procedure, only the resistance of the wire is measured from both supplied voltage and current. This provides the mean wire temperature knowing the TCR after a calibration in an oven, confirming standard value of 3.85 10^{-3} K^{-1}. The location of the contact point is the centre of the wire (x = 0) for which the temperature must be known. When the thermocouple temperature equals the contacted wire temperature, its temperature distribution is identical to the non-contact, with a shape close to a parabola (see Fig. 10). When solving a linear differential equation (materials thermal characteristics independent from temperature and no radiative heat transfer), the solution is a parabola for which the ratio between the maximum central temperature and the mean wire one is 3/2. In the present case, by taking account of the thermal dependence of resistivity and the radiative heat transfer, the parabola is slightly distorted so that the ratio changes too. As a result, after having verified the validity of the model by comparing measured and calculated mean wire temperatures, we assume that the central point temperature can be deduced from the model. In Fig. 11, measurements points are depicted and superimposed to the calculated ones (curved lines). In this figure, measurements points are mean values in blue for which the difference with the calculated curve never exceeds 3 K (point size in this figure). This confirms the reliability of the calculations so that measurement points of the centre values have been extrapolated from the ratio between blue and orange line, given by the model. The ratio between centre and mean temperature is also plotted in the same graph (black dotted line). As a result, we assume that the central point temperature can be deduced from the model.

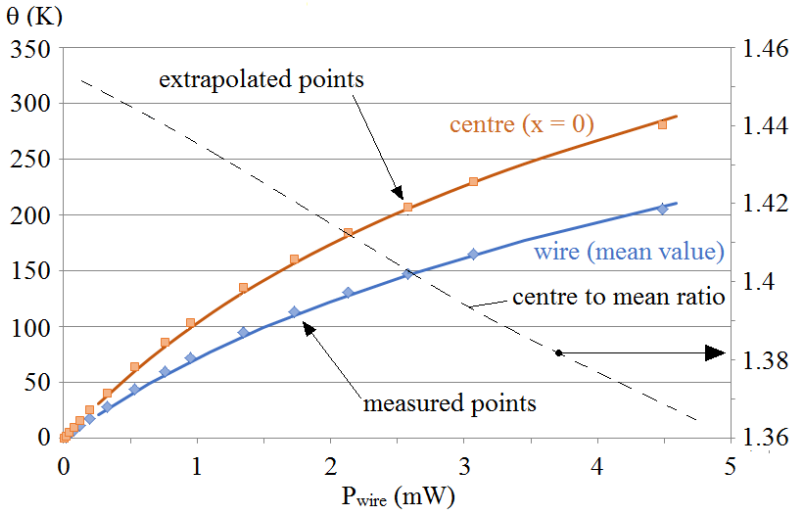

Fig. 11. Comparison between measurement points and modelling (curve) of the mean wire temperature in blue colour. Centre temperature is provided by the model from which the points have been extrapolated (orange colour) using ratio values depicted by the black dotted line.

In the following results, contact wire temperatures are extrapolated from the same ratio on measured mean values.

5. Experimental setup

The thermocouple junction must be put in contact with the platinum wire for the calibration procedure. This wire is supplied with a DC current for heating purpose and the thermocouple is supplied with an AC current for the same reason. Since an electrical contact between them may generate electrical interferences, a little pad of isolating material was deposited by means of the FIB technique. This pad is clearly visible in Fig. 8 that shows two different images at two different magnifications. In the image on the left (Fig. 12a), with a magnification of 526 and a scale of 20 µm, we can clearly see the platinum wire with a diameter of 20 µm in white, with the triangle formed by the thermocouple also in white but with a diameter of about 1.2µm.

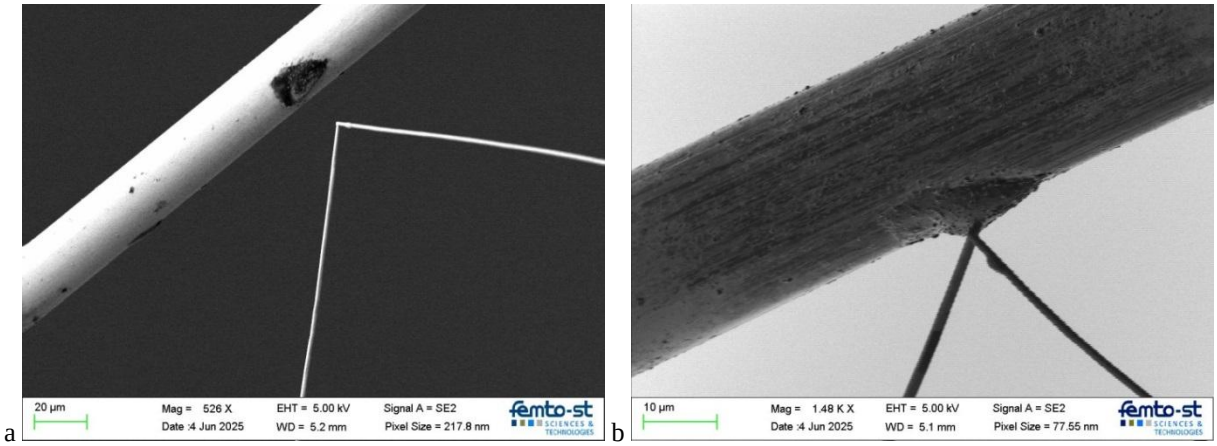

a b

Fig. 12. Calibration Platinum wire and micro-thermocouple views. Isolating pad deposited using FIB is visible (a), on which the thermocouple can be put in contact (b) by means of a micro-robot [1].

On the thick platinum wire, just opposite the tip of the thermocouple, which is not yet in contact, we used the Ion Beam Assisted Deposition (IBAD) method to create a thin layer of naphthalene on an elliptical surface measuring 5 x 15 µm². Naphthalene is introduced into the microscope chamber via a Gas Injection System (GIS) equipped with three gas cartridges: xenon fluoride (XeF2), cyclopentadienyl platinum (Pt-based) and naphthalene (C-based) from Oxford Instruments, type OmniGIS. The gas injector is retractable and removable so that the nozzle can be positioned as close as possible to the area to be covered. We injected a small amount of gaseous naphthalene into the chamber using a syringe placed less than 100 µm from the area to be covered, the pressure in the line of gas and the nozzle is around 4×10^{-2} mbar, so that the total pressure in the chamber did not rise above 5×10^{-6} mbar. With the Focused Ion Beam (FIB), we sputter the surface to be coated with a low FIB beam of 5µA/µm² of gallium, in order to stimulate the surface

and make it reactive, while at the same time breaking down the gas molecules to help them condense on the activated surface. Because the surface of the reference wire is not flat, the thickness of the layer is not homogeneous.
In Fig. 12b, the picture magnified 1480x with a scale of 10 µm, shows the thermocouple in contact with the naphthalene deposit, which forms a small bump on the platinum reference wire. This carbon and hydrogen-based deposit is an electrical insulator that allows us to clearly separate the two electrical signals from the platinum reference wire and the thermocouple in active AC mode, without providing too much thermal insulation, since the thickness of the naphthalene deposit is around 3 µm. The contact point between the thermocouple in active AC mode and the naphthalene represents an area of less than 1 µm², which allows for very high measurement accuracy and reproducibility. The heat exchange zone is located at the centre of the naphthalene deposit, where its thickness is the greatest.
Through the numerous series of measurements, we were able to perform, with and without naphthalene deposition, we observed that adding naphthalene to the platinum wire in DC mode improves and effectively isolates the two electrical signals across the entire temperature range without disrupting heat exchange. Naphthalene enabled us to eliminate interference between the AC and DC electrical signals between the wire and the thermocouple in active mode.

For heating the thermocouple (active thermometry), we applied a sinusoidal current at radial frequency ω. The resulting Joule heating produces a power modulation at 2ω, leading to a temperature variation at 2ω and a DC offset. The thermal cutoff frequency of such a thermocouple lies in the range 450–900 Hz, depending on the surrounding medium and the heating source. At higher frequencies, the 2ω component magnitude vanishes, whereas the DC component remains.
In the null-point method, only the DC component of the temperature, which is influenced by the tip–sample contact, is measured. Some authors drive the input current at frequencies well above the thermocouple cut-off, typically around 100 kHz. However, such high frequencies can introduce detrimental capacitive and inductive effects across the devices, cables, and components, which must be mitigated with appropriate filters and amplifiers. For this reason, we used a frequency of only 5 kHz, which is sufficient to provide relevant measurements.
Several strategies exist to suppress the parasitic DC component from the power supply and the 1ω voltage at the thermocouple output, much larger than the thermal DC signal of interest. A Wheatstone bridge can address both issues but requires frequent equilibration. Higher harmonics (2ω and above) may remain and have magnitudes similar to the Seebeck DC component, potentially altering the voltmeter reading depending on its sensitivity. Another approach to remove the parasitic DC component is to place a capacitor between the voltage generator and the thermocouple. The unwanted 1ω component (and higher frequencies) can be substantially reduced with a low-pass filter.
For simplicity, we selected the second method. Fig. 13 illustrates the electrical setup: a capacitor C_0 removes any DC component from the function generator V_{in}, a resistor R_0 for current measurement, and two RC low-pass filter stages.

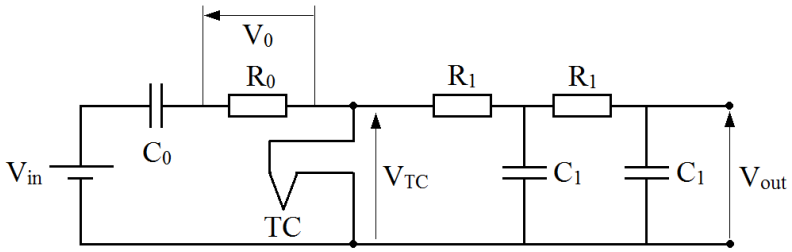

Fig. 13. Electrical setup; R_0 = 336 Ω ; C_0 = 220 µF ; R_1 = 100 kΩ ; C_1 = 2.2 µF.

In this figure, TC represents the thermocouple, whose resistance is near 100 Ω. Three precision voltmeters measure the relevant signals: V_0 (AC), V_{TC} (AC), and V_{out} (DC). The input AC voltage V_{in} ranges from 0 to 600 mV, yielding a thermocouple maximum current typically of 1.3 mA and a junction temperature rise of about 250 K. The dissipated power through the thermocouple can be determined using V_{TC}, in the range 0-200 mV, at the input frequency (5 kHz) without filtering. At this frequency, the second and third harmonics (2ω and 3ω) related to Seebeck and resistivity effects are reduced to a level that is negligible compared with the fundamental 1ω component. The two-stage first order filter provides the remaining DC output V_{out} of the thermocouple that represents the steady temperature of the junction due to Seebeck effect.

6. Results and discussion

Three different levels of wire temperatures have been used in the following results. For each of these three levels, both wire and thermocouple data have been recorded as the Joule power in the thermocouple varies. Fig. 14 depicts the

results, showing measurement points and their fitting linear equations. For each series, the thermocouple was in contact with the wire and the linear increase of its temperature is clearly visible. Here, the wire temperatures are the extrapolated central values from the measured mean ones without taking into account of the possible thermocouple contact disturbance. However, this is not a problem since the crossing point of interest is not affected by the contact due to thermal equilibrium between thermocouple junction and the wire surface. As a result, if the central temperature would be significantly affected, only the slope would change but not the crossing point location. Without any effect, the slope would be in theory null. The remaining tiny slope shown in Fig. 14 demonstrates that the contact effect is weak but measurable. The wire temperature slightly increases when the thermocouple junction temperature increases due to heat exchange through the contact. When the temperatures are the same, the heat transfer vanishes: the wire is no more perturbed and the crossing points provide the actual contact temperatures, using extracted equations. It is interesting to note that the slopes of thermocouple junction temperatures are different. This means that the thermal contacts are different due to different contact strength and/or geometrical contact. Indeed, between each measurement series, the thermocouple was pulled off from the wire pad surface.

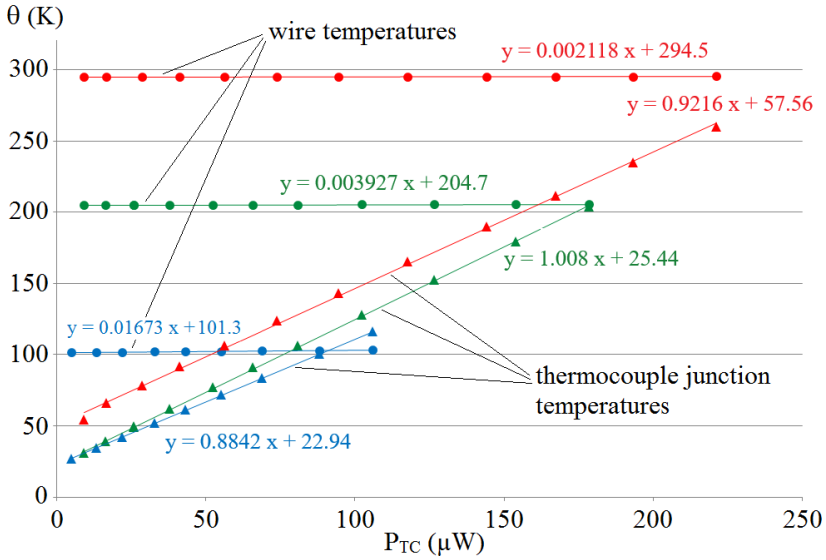

Fig. 14. Experimental points obtained at three different heating power of the calibration wire versus Joule power thermocouple heating (P_{TC}). Wire temperatures are the extrapolated central point where the thermocouple junction is in contact on the isolating pad.

As it was shown in the theoretical analysis, if the contact conductance is constant the junction temperature must increase linearly. As shown in Fig. 7, this linearity is not perfect when the temperature range is important. This is confirmed in Fig. 14 for the largest range of measurement points (red triangle). Since the slight curvature appears both with and without contact, the origin cannot be attributed to a variation in contact conductance. Indeed, the thermal expansion of the thermocouple could cause this variation in contact by increasing the contact force. However, taking account of linear thermal expansion coefficient of the order of 9 μK^{-1} for platinum (8 μK^{-1} for rhodium), the increase of a 300 µm length wire gives 2.7 $nm.K^{-1}$. We have measured a mean displacement of the junction of 2.25 nm.K-1 which is coherent. This effect is therefore not susceptible to change the contact conductance significantly, especially on a long and free of constraint calibration wire.

The deduced temperature elevations of the wire (crossing points) are 102.8, 205.4 and 295.1 K for a wire heating power of 0.88, 2.37 and 4.63 mW respectively. These temperatures are located at the centre point of contact, deduced from the mean measured values. Based on these values, we have extracted the thermocouple data to deduce contact temperatures at these three levels. Fig. 15 shows the measured points in five different situations: no contact (black), cold contact (red) and hot contacts on wire at 102.8 K (blue), 205.4 K (yellow) and 295.1 K (green). Each series of points have been fitted by the least squares method for extracting its linear equation.

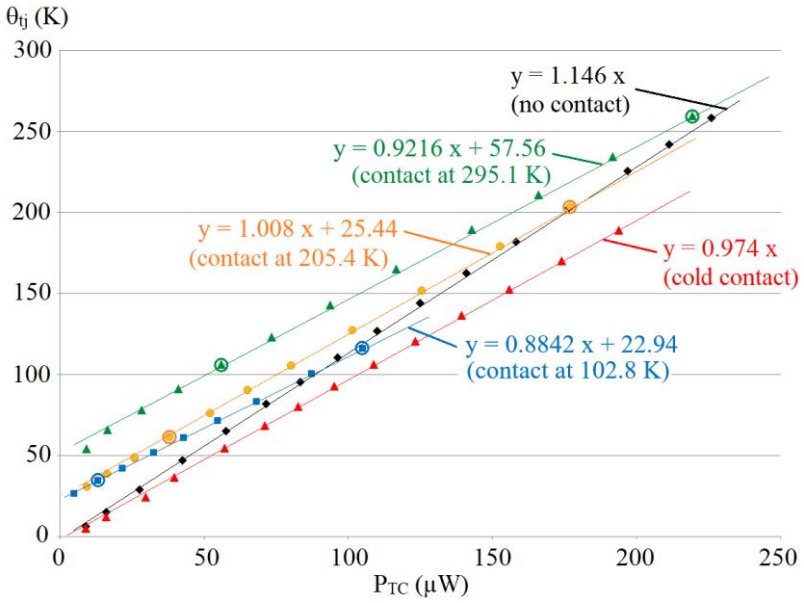

Fig. 15. Measured temperature at the contact point from the thermocouple versus power supplied in different configuration of no-contact (black), cold contact (red) and hot contact at three levels of wire temperatures (blue, yellow and green).

From these results, we have calculated the crossing points temperatures using two methods: the extracted slopes from all points (see equations in Fig. 15) and the use of only two measurements points (in circles in Fig. 15) as shown in Table 2.

Table 2. Deduced surface temperature elevations.

Wire centre temperature		102.8 ± 3 K	205.4 ± 3 K	295.1 ± 3 K
Method	Slope on all points (WLS fitting)	100.3 ± 0.9 K	211.2 ± 4.4 K	293.7 ± 3.5 K
	Slope on 2 points	100.1 ± 2 K	210.5 ± 6.6 K	296.2 ± 5 K

Deduced temperatures are in good agreement with the calculated wire temperatures, showing that the simplest two points method is sufficient to obtain a relevant value.

Thermocouple measurement uncertainties depend on the thermocouple itself and the electronic used in active mode. Temperature uncertainty of a S-type thermocouple is known to be in the range of a half degree. Low-pass filter allows reducing significantly noise and disturbances so that the DC output voltage should not be affected. The thermoelectric voltage is stable in the range of ± 1 µV. However, voltmeters used to provide the supplied power can slightly be disturbed or deviates from actual values. As a result, measurements global uncertainties are quite low so that the final uncertainty on the crossing point location stays mainly depending on the slope difference between the non-contact and hot-contact temperature response. However, in our measurements, the calculated uncertainties remain below 7 K, even with 2 computation points.

One can notice that the largest difference between wire and measured values corresponds to the second values (wire at 205.4 K) for which the two slopes are the nearest (1.008 for hot contact compared to 1.146 for non-contact). It is worth mentioning that any slope deviation due to uncertainties has a minimum influence for the angle between the two curves approaching $\pi/2$. On the contrary, the effect increases when the angle between the fitted hot contact and non-contact lines decreases. As a consequence, the reliability of the results is better for larger thermal contact conductance g.

Actual values of contact conductance g are noted as g_c is the simple 0-D model. Even if experimental results are remarkably linear, this model cannot be used to calculate external conductance g_e and contact conductance g_c. This is due to the complex combination of temperature dependence of the different material properties all along the wires in addition to the consideration of radiative heat transfer and the resulting asymmetrical distribution temperature along the thermocouple wires. In Fig. 16, the measurement points have been fitted using the model of section 2.2, providing the best fitting results with g contact conductances as indicated. One can notice that contact conductance can vary by a factor of 2, between 0.06 to 0.12 µW K^{-1}.

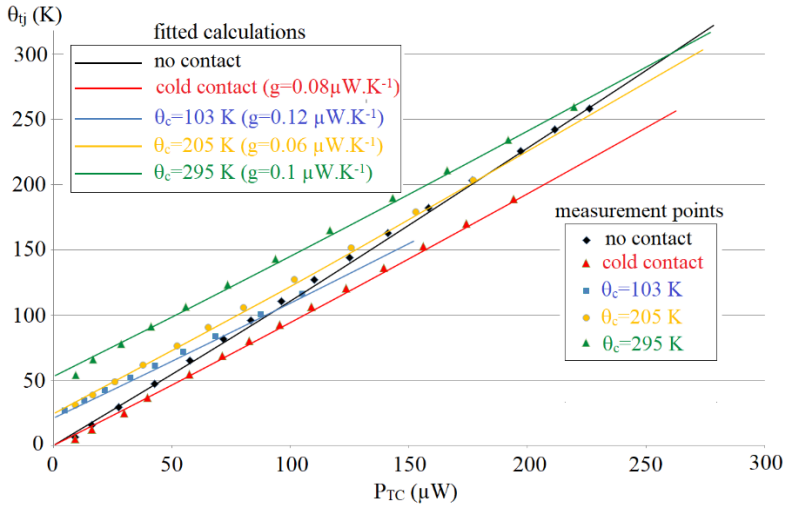

Fig. 16. Comparison between measurement and modelling giving the best fitting values of contact conductance g.

7. Conclusion

We have shown a new simplified vacuum null-point method, which needs only one scan with two successive measurements at different Joule heating powers. We employed as a sensor a thermocouple wire whose hot junction was rectified with a FIB. However, this procedure could be applied with a standard SThM probes. We modelled both the thermocouple and a calibration device consisting of a platinum wire. Using the fact that we know the temperature of the platinum wire, we used it to validate the new VNP procedure. The uncertainties are better than 10 K even at high temperatures.

The key point of the proposed method relies on the linearity of the junction temperature versus the supplied Joule power to the thermocouple. This linearity persists when a contact occurs, only the slope changes regarding the contact conductance. Consequently, the slope extraction using at least two points allows to obtain a crossing point with non-contact linear fit that provides the contact temperature. Compared to previous published VNP, there is only one scan therefore there is no change of conductance between two scans. To increase the reliability of the contact temperature, the slight deviation from the linearity could be investigated and taking into account in a future work.

Furthermore, an increase of the contact conductance would benefit to the reliability of the crossing point extraction due to a lower slope. For this purpose, a larger contact surface using for instance a larger thermocouple size can be considered.

In wire thermocouple, Joule heating occurs on the whole wire length. Consequently, their use in ambient pressure environment is not easy due to the large amount of heat exchange all around the probe and with the surface. As a result, the thermal balance between the junction and the surface at equilibrium is not only due to the contact heat exchange and the resulting obtained surface temperature is wrong. This is a problem that we have to address in our upcoming works.

7. Acknowledgments

This work has been partly supported by the French research infrastructure ROBOTEX (TIRREX ANR-21-ESRE-0015) and its FEMTO-ST technological facility CMNR, (Center of Micro and Nano Robotics). The authors acknowledge the support of the French RENATECH network.

The author thanks the EUR EIPHI (grant number ANR-17-EURE-0002), The National Agency of Research (ANR), the French 2030 program, the University Marie and Louis Pasteur and the region Bourgogne-Franche-Comté for financial support during this study.

The author thanks also, Supmicrotech ENSMM, engineers' school for all the facilities and location, UTBM and the CNRS for other supports.

References

[1] L. Thiery, J.Y. Rauch, Y. Lei, High resolution surface contact temperature measurements by means of micro-thermocouples in vacuum conditions, Int. J. Thermal Sci. 195 (2024) 108663; https://doi.org/10.1016/j.ijthermalsci.2023.108663.

[2] Yifan Li, Yuan Zhang, Yicheng Liu, Huaqing Xie & Wei Yu, A Comprehensive Review for Micro/Nanoscale Thermal Mapping Technology Based on Scanning Thermal Microscopy Journal of Thermal Science volume 31, pages976–1007 (2022), DOI: 10.1007/s11630-022-1654-1.
[3] S. Gomes, A. Assy and P-O. Chapuis, Scanning thermal microscopy: A review Phys. Status Solidi A 212, No. 3, 477–494 (2015) / DOI 10.1002/pssa.201400360.
[4] K. Kim, J. Chung, J. Won, O. Kwon, J.S. Lee, S.H. Park and Y.K. Choi, Quantitative scanning thermal microscopy using double scan technique, Appl. Phys. Lett. 93, 203115 (2008), DOI: 10.1063/1.3033545.
[5] K. Kim, J. Chung, G. Hwang, O. Kwon and J.S. Lee, Quantitative measurement with scanning thermal microscope by preventing the distortion due to the heat transfer through the air, ACS Nano 5, 8700-8709 (2011), DOI: 10.1021/nn2026325.
[6] J. Chung, K. Kim, G. Hwang, O. Kwon, S. Jung, J. Lee, J.W. Lee, G.T. Kim, Quantitative temperature measurement of an electrically heated carbon nanotube using the null-point method, Rev. Sci. Instrum. 81 (2010) 114901; doi: https://doi.org/10.1063/1.3499504.
[7] J. Chung, K. Kim, G. Hwang, O. Kwon, Y.K. Choi, J.S. Lee, Quantitative temperature profiling through null-point scanning thermal microscopy, Int. J. Therm. Sci. 62 (2012) 109–113, https://doi.org/10.1016/j.ijthermalsci.2011.11.012.
[8] G. Hwang, J. Chung, O. Kwon, Enabling low-noise null-point scanning thermal microscopy by the optimization of scanning thermal microscope probe through a rigorous theory of quantitative measurement, Rev. Sci. Instrum. 85 (2014) https:// doi.org/Artn 11490110.1063/1.4901094.
[9] J. Cha, H. Shin, O. Kwon, Vacuum null-point scanning thermal microscopy: Simultaneous quantitative nanoscale mapping of undisturbed temperature and thermal resistance, International Journal of Thermal Sciences 172 (2022) 107268, DOI: https://doi.org/10.1016/j.ijthermalsci.2021.107268.
[10] T.P. Nguyen, L. Thiery, S. Euphrasie, E. Lemaire, S. Khan, D. Briand, L. Aigouy, S. Gomes and P. Vairac, Calibration tools for Scanning Thermal Microscopy probes used in temperature measurement mode, J Heat Transfer 141(7) 071601 (2019); HT-18-1667, doi: 10.1115/1.4043381.
[11] T.P. Nguyen, L. Thiery, S. Euphrasie, S. Gomès, B. Hay, and P. Vairac, Calibration of thermocouple-based scanning thermal microscope in active mode (2ω method), Rev. Sci. Instrum. 90, 114901 (2019), doi: 10.1063/1.5119044.
[12] L. Thiery, E. Gavignet and B. Cretin, Two omega method for active thermocouple microscopy, Rev. Sci. Instrum. 80, 034901 (2009).
[13] C.Y. Ho, R.W. Powell and P.E. Liley, Thermal Conductivity of the Elements, Journal of Physical and Chemical Reference Data 1, 279 (1972); https://doi.org/10.1063/1.3253100.
[14] J.W. Arblaster, Selected Electrical Resistivity Values for the Platinum Group of Metals Part I: Palladium and Platinum, Johnson Matthey Technol. Rev., 2015, 59, (3), 174–181; http://dx.doi.org/10.1595/205651315X688091.
[15] Derek York, Least-squares fitting of a straight line, Canadian Journal of Physics (44) 5, (1966); https://doi.org/10.1139/p66-090.
[16] Michael H. Kutner *et al.*, "Applied Linear Statistical Models" 5th ed, McGraw-Hill, Irwin, New York (2005).